

Location of the dsRNA-Dependent Polymerase, VP1, in Rotavirus Particles

Leandro F. Estrozi¹, Ethan C. Settembre², Gaël Goret³, Brian McClain⁴, Xing Zhang⁵, James Z. Chen⁵, Nikolaus Grigorieff⁵ and Stephen C. Harrison⁶

1 - European Molecular Biology Laboratory, Grenoble Outstation, 6 Rue Jules Horowitz, Grenoble 38042, France

2 - Laboratory of Molecular Medicine, Children's Hospital, Boston, MA 02115, USA

3 - Institut de Biologie Structurale, UMR 5075, Centre National de la Recherche Scientifique, Grenoble F-38027, France

4 - Department of Molecular and Cellular Biology, Harvard University, Cambridge, MA 02138, USA

5 - Rosenstiel Basic Medical Sciences Research Center and Howard Hughes Medical Institute, Brandeis University, Waltham, MA 02454, USA

6 - Harvard Medical School, Children's Hospital, and Howard Hughes Medical Institute, 3 Blackfan Circle, Boston, MA 02115, USA

Correspondence to Leandro F. Estrozi and Stephen C. Harrison: estrozi@embl.fr; harrison@crystal.harvard.edu
<http://dx.doi.org/10.1016/j.jmb.2012.10.011>

Edited by M. Moody

Abstract

Double-stranded RNA (dsRNA) viruses transcribe and replicate RNA within an assembled, inner capsid particle; only plus-sense mRNA emerges into the intracellular milieu. During infectious entry of a rotavirus particle, the outer layer of its three-layer structure dissociates, delivering the inner double-layered particle (DLP) into the cytosol. DLP structures determined by X-ray crystallography and electron cryomicroscopy (cryoEM) show that the RNA coils uniformly into the particle interior, avoiding a “fivefold hub” of more structured density projecting inward from the VP2 shell of the DLP along each of the twelve 5-fold axes. Analysis of the X-ray crystallographic electron density map suggested that principal contributors to the hub are the N-terminal arms of VP2, but reexamination of the cryoEM map has shown that many features come from a molecule of VP1, randomly occupying five equivalent and partly overlapping positions. We confirm here that the electron density in the X-ray map leads to the same conclusion, and we describe the functional implications of the orientation and position of the polymerase. The exit channel for the nascent transcript directs the nascent transcript toward an opening along the 5-fold axis. The template strand enters from within the particle, and the dsRNA product of the initial replication step exits in a direction tangential to the inner surface of the VP2 shell, allowing it to coil optimally within the DLP. The polymerases of reoviruses appear to have similar positions and functional orientations.

© 2012 Elsevier Ltd. All rights reserved.

Introduction

Double-stranded RNA (dsRNA) viruses do not release their genomic RNA when they enter a cell. Instead, for each genomic segment, they package a dsRNA-dependent RNA polymerase, which transcribes the segment into mRNA and exports the product from the particle. Like most other mammalian dsRNA viruses, rotavirus particles have a multilayer protein shell.¹ The virion is a “triple-layered particle” (TLP); the transcriptionally active,

inner capsid particle is a “double-layered particle” (DLP). The role of the outer protein layer, which includes the proteins VP4 (cleaved to VP8* and VP5*) and VP7, is to attach virions to the cell surface and to deliver the DLP into the cytosol.¹

The DLP contains four protein species: VP2 (120 copies), assembled into a thin but tightly packed shell surrounding the RNA; VP6 (780 copies), arrayed as 260 trimers on the outer surface of the VP6 shell; VP1 (11 or 12 copies), the dsRNA-dependent RNA polymerase enclosed along with the

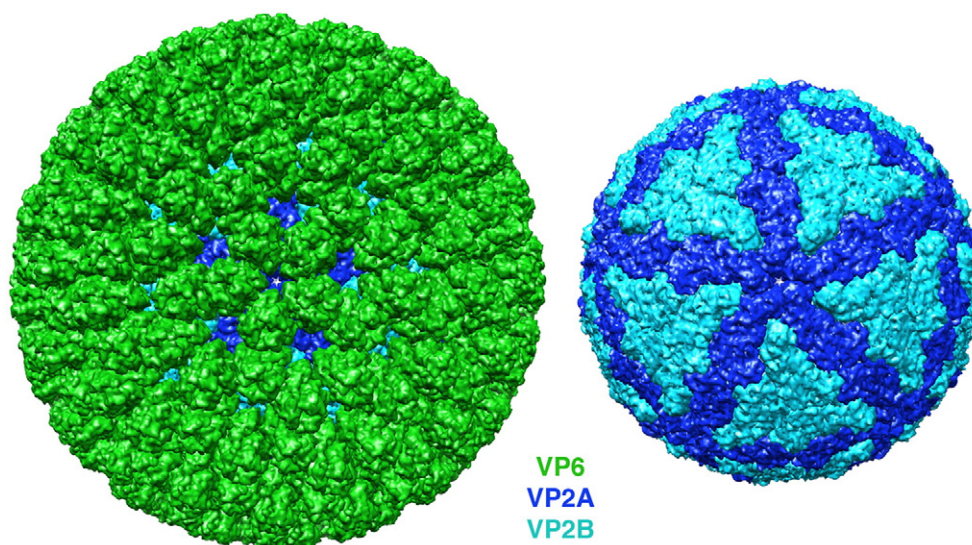


Fig. 1. Surface views of the rotavirus DLP (left) and the VP2 inner layer (right). VP6 is in green, and the conformers of VP2 (VP2A and VP2B) are in dark blue and cyan, respectively. The view is along a 5-fold axis. Note that small gaps in the VP6 layer allow the VP2 layer to show from beneath.

11 dsRNA segments within the VP2 shell; and VP3 (11 or 12 copies), the mRNA capping enzyme, likewise enclosed within the VP2 shell. **Figure 1** shows the organization of VP2 and VP6, the icosahedrally symmetric components, from the structure of the DLP as determined by X-ray crystallography.² Each icosahedral asymmetric unit contains two chemically identical VP2 subunits (designated VP2A and VP2B), having closely related conformations but making completely distinct inter-subunit contacts. The VP2A subunits encircle the fivefold positions; the VP2B subunits insert into gaps in the VP2A ring distal to the fivefold. The (VP2A–VP2B)₅ decamer is probably the assembly unit of the VP2 shell.^{2–4} The well-ordered VP2A chain trace begins at residue 100 and continues to the end of the polypeptide chain at residue 880; the ordered VP2B chain trace begins at residue 81. The 80- to 100-residue N-terminal “arms” of both VP2 conformers project toward the fivefold (**Fig. 2**).

The 11 dsRNA genomic segments appear to coil tightly inside the VP2 shell, generating a series of concentric, low-resolution density layers after icosahedral averaging.^{2,5,6} These layers avoid a region around the fivefold, which contains a set of rod-like density features. In the original interpretation of the X-ray crystallographic density map, some of these features were ascribed to the N-terminal arms of VP2, with the suggestion that they contribute to a “fivefold hub”.² One of us (L.E.) has examined those features in an improved electron cryomicroscopy (cryoEM) reconstruction of the DLP and shown that VP1, in five equivalent orientations, fits the density with excellent fidelity, including the density close to the 5-fold axis, which is a superposition of five VP1

densities (each at 20% occupancy).⁶ As reported here, we have reexamined the X-ray map and arrive at precisely the same interpretation. We further show that a cryoEM reconstruction of the TLP has similar VP1-derived features but displaced radially inward by about 10 Å, consistent with changes previously detected in the VP2 and VP6 layers, when the outer-layer proteins are added.^{7,8} We describe the functional consequences of the position and orientation of VP1 confirmed by examination of these various independently derived maps. Zhang *et al.* have drawn comparable conclusions from a closely related assignment of density to the dsRNA-dependent RNA polymerase ($\lambda 3$) in a 7-Å-resolution cryoEM map of an orthoreovirus.⁹

Results

Locating VP1 in the DLP cryoEM reconstruction

We calculated an improved reconstruction of the rotavirus DLP, at an estimated resolution of 4.2 Å, applying the symmetry-adapted functions (SAFs) procedure⁶ to the images used to generate the previously reported DLP structure.⁵ The cryoEM reconstruction shows a readily interpretable hub of density features near the 5-fold axis, just within the VP2 shell (**Fig. 2**). The ratio of the density in this fivefold hub to the density in the VP2 and VP6 shells is about 0.17, consistent with the assumptions that the distinct features represent the average of a single copy of VP1 in five equivalent positions and that other contributions (from the N-terminal arms of VP2, which also occupy some of this volume, and

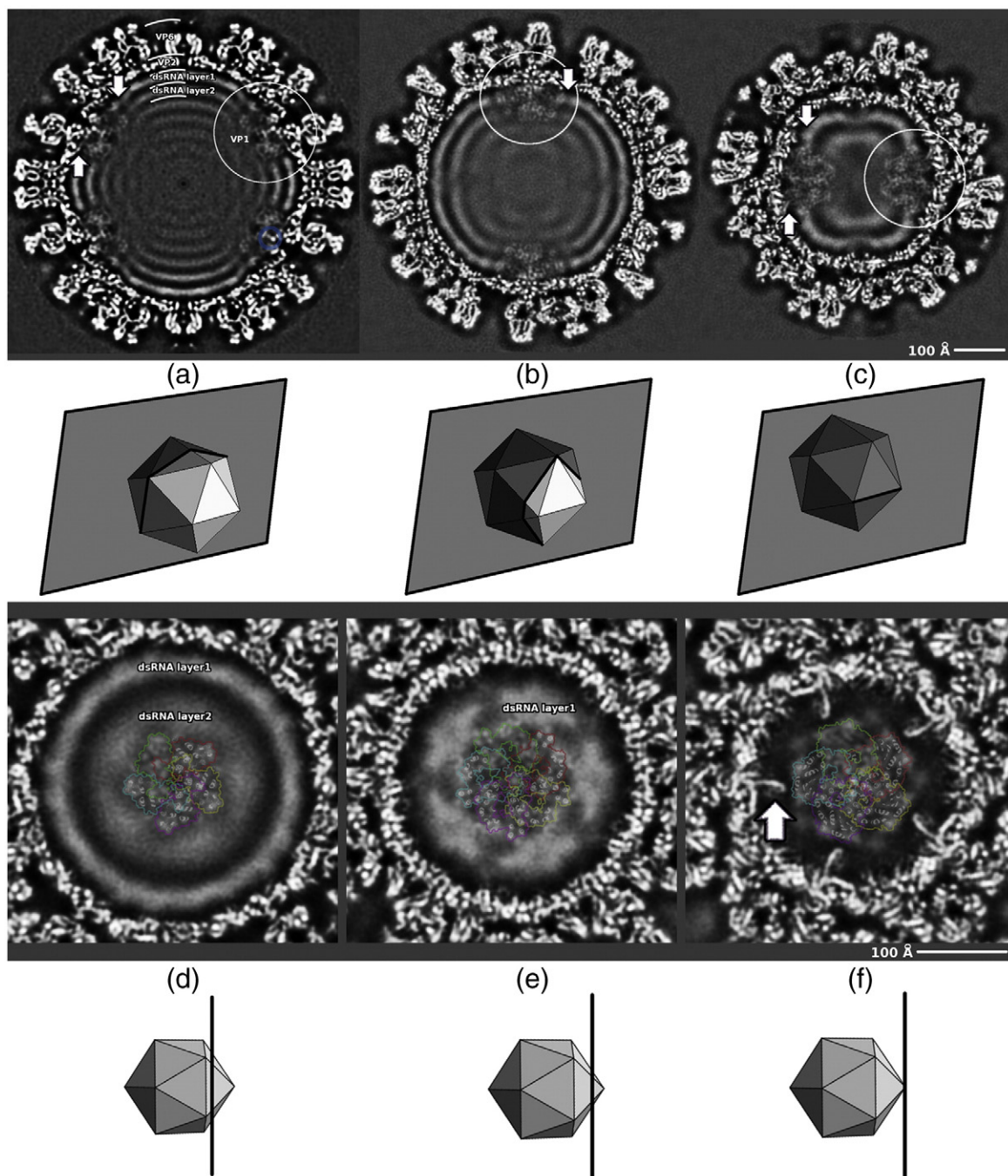


Fig. 2. Cross-sections through reconstructed DLP density map, calculated with SAFs to a nominal resolution of 4.2 Å (FSC=0.143 criterion). Beneath each panel is a diagram showing the orientation and position of the section with respect to icosahedral symmetry axes as a semitransparent plane cutting an icosahedron. (a–c) Sections normal to a 2-fold axis. (a) Section passes through DLP center; (b) section cuts two vertically aligned 5-fold axes; (c) section normal to 2-fold axis and intersecting two horizontally aligned 5-fold axes. Densities associated with VP1 are indicated by white circles. The upward arrows indicate VP2 N-terminal arms “holding” VP1, and the downward arrows indicate the contact between VP1 and the first RNA layer. (d)–(f) Sections normal to a 5-fold axis. Coordinates of VP1 fitted to the density are shown as light-gray ribbons (overlay) at four of the five equivalent positions occupied by VP1, showing the match between secondary-structure elements of VP1 and rod-like densities in the EM map. The outer contour of each VP1 position is in color, showing overlap between neighboring VP1 positions. One position (green) left with no ribbons to show EM density more clearly.

potentially from RNA) are effectively uniform. The lower occupancy of protein in the fivefold hub and the likely overlap with disordered structures (e.g., the VP2 N-terminal arms) diminish the effective resolution in that region, which we estimate (based on the appearance of α -helices, etc.) to be between 5 and 6 Å.

There are a number of rod-like features in the fivefold hub, particularly in regions displaced from the axis. Fitting the VP1 coordinates⁴ into these features, while taking into account the weighted sum of contributions to the overlap volume,¹⁰ yielded a convincing and unambiguous match⁶ (Fig. 3a). The centroid of VP1 is offset from the symmetry axis so that the five equivalent images of VP1 overlap only near the 5-fold axis. The fit is particularly well defined because much of the protein does not overlap fivefold-related images of other well-defined density. Strong features near the fivefold are superpositions of secondary-structure elements in two or more of the five equivalent orientations of VP1. For example, the radially directed rods, previously interpreted as α -helices when interpreting the X-ray crystallographic density map (see Fig. 9b in Ref. 2), are superpositions of an α -helix (residues 32–51) and a β -strand (residues 747–754), both radially oriented.

Locating VP1 in the X-ray crystallographic electron density map

We confirmed the fit of VP1 into the cryoEM image reconstruction by an independent analysis of the electron density map derived by X-ray crystallography.² A map calculated with terms cut off beyond 5 Å resolution was the clearest of those we examined. A helix–turn–helix feature, with strong connectivity in the turn, provided a good starting point. Analysis of the VP1 structure showed only one pair of sequence-adjacent helices that matched in length and relative orientation: one helix contains residues 282–298; the other, residues 301–312. A model placed to fit these helices into the helix–turn–helix density placed additional helices in or near suitable

density features, and simple rigid-body shifts aligned all the main features of VP1 (or their fivefold averages in the overlap region) with corresponding density (Fig. 3b).

Locating VP1 in the TLP

The TLP cryoEM image reconstruction⁸ has density features corresponding closely to the VP1 density in the DLP, but the entire set of features, along with the tip of VP2A, has shifted inward (Figs. 3c and 4). The displacement is consistent with previously analyzed changes in the VP2 shell that accompany binding of VP7 to the tip of VP6: addition of VP7 alters the radial tilt of peripentadal VP6 trimers, pushing inward on the loops of VP2 abutting the fivefold.

VP1–VP2 contacts

The placement of VP1 in density as just described creates a largely complementary interface between it and the VP2 shell (Fig. 4). There are three positions of minor overlap: first, where the VP2A helix–loop–helix that defines the pore around the 5-fold axis (residues 341–370) collides with residues 968–980 of VP1; second, where the same segment of a fivefold-related VP2A (the counterclockwise neighbor when viewed from outside the shell) overlaps residues 1022–1025 of VP1; and third, where residues 337–338 of the latter VP2A comes close to a turn at residues 264–267 of VP1. At all three positions, modest adaptations in either partner could alleviate any clash. In addition, some part of VP2A must shift during transcription to allow RNA to exit, as the pore at the 5-fold axis of the non-transcribing DLP is too narrow to accommodate an RNA strand.² The N-terminal densities of two adjacent VP2A subunits (residue 100) and a VP2B (residue 81) about the VP1 model. The X-ray map suggests that, in the other four of the five VP2B subunits, the helix that begins at residue 81 in the DLP model might extend for another 2–3 turns in an N-terminal direction. Moreover, the full-strength density in the X-ray map at residue 100

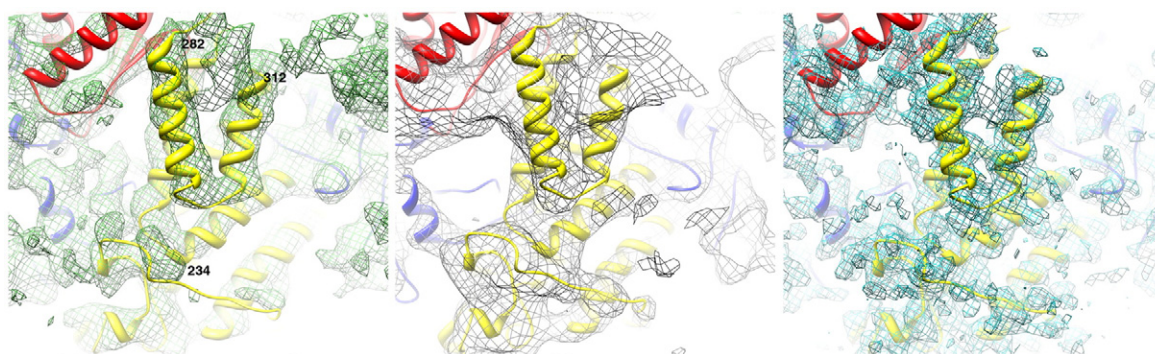


Fig. 3. Fit of VP1 model to density. (a) DLP cryoEM map as in Fig. 2; (b) X-ray map²; (c) TLP cryoEM map.⁸

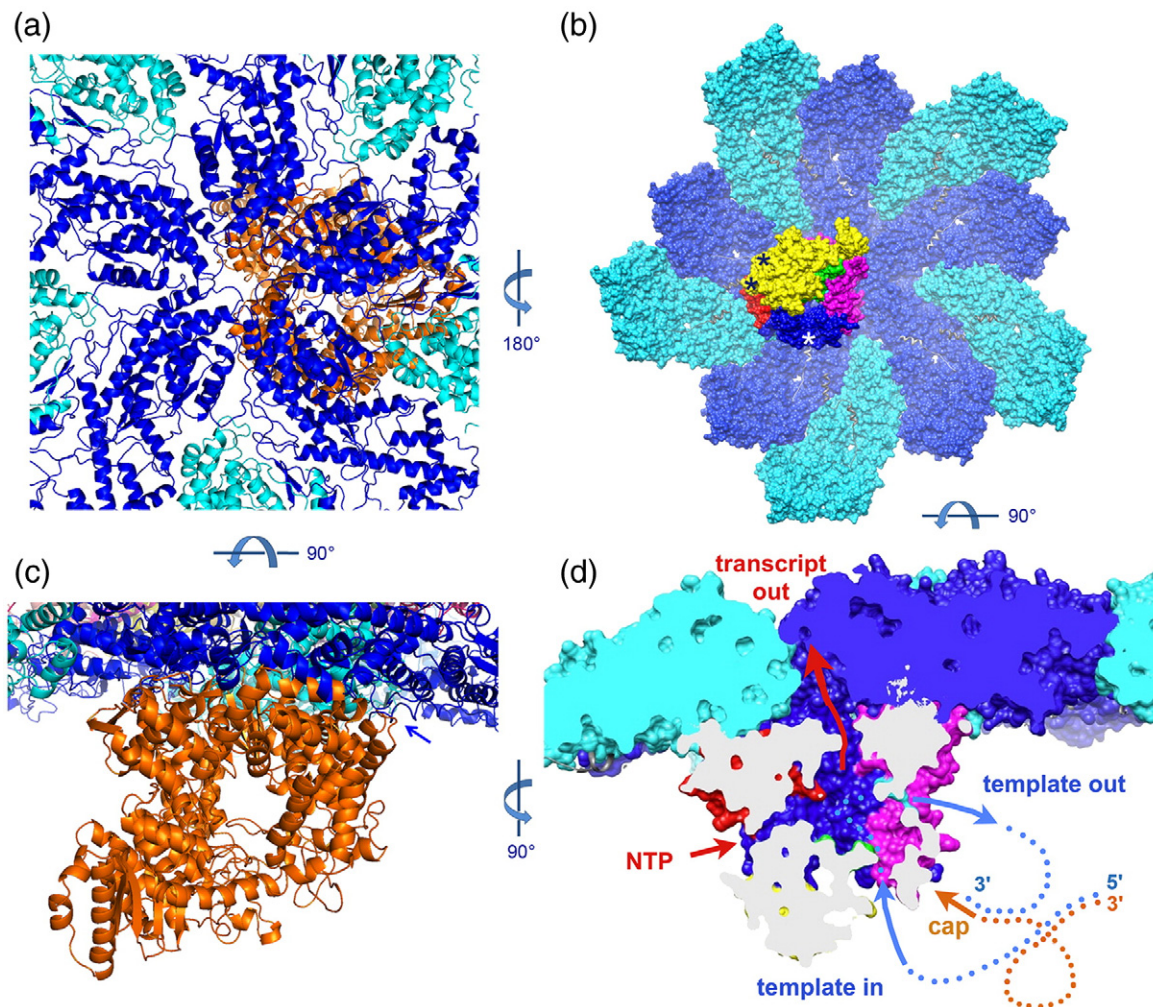


Fig. 4. Functional orientation of VP1. (a) Ribbon representation of the placement of VP1 (orange) with respect to VP2A (blue) and VP2B (cyan), viewed along a 5-fold axis from outside the VP2 shell. (b) Surface representation of 10 VP2 subunits surrounding a 5-fold axis, colored as in (a), and the associated VP1, viewed from inside the DLP. The domains of VP1 are colored yellow (N-terminal domain), green (fingers subdomain), red (palm subdomain), blue (thumb subdomain) and magenta (C-terminal domain). The positions at which N-terminal arms of three different VP2 subunits clearly contact the VP1 shown are marked by asterisks; the remaining N-terminal arms may also contact this VP1 molecule, but their density overlaps that of its fivefold “ghosts”. (c) As in (a), but viewed in a direction tangential to the VP2 shell, looking into the template (and dsRNA) exit channel of VP1. Arrow indicates contact between VP1 and the N-terminal arm of a VP2A subunit. (d) Representation as in (b), but viewed in a direction tangential to the VP2 shell and normal to the view in (c), cut away to show the internal cavity in VP1 that contains the catalytic site. The channels leading into this cavity are labeled. The dashed curves and arrows show schematically (not to scale) how the minus-sense strand of the genome (blue) threads through the polymerase, leaving a “transcription bubble” in the plus-sense strand (orange), the latter anchored to the polymerase by its 5′ cap.

in VP2A and at residue 81 in VP2B shows that N-terminal arms of all 10 VP2 subunits penetrate into the fivefold hub region. The arms are evidently flexible tethers for VP1 and VP3, as they are necessary for incorporation of those components into assembling particles.¹¹

Association with VP2 activates VP1.^{3,12} A contribution to the presumed conformational change that activates the polymerase might come from the interaction of the N-terminal arm of VP2B with the

surface of VP1. The contact occurs at a site that contains residues just distal to the “priming loop” (residues 492–498) and also residues just distal to the Asp-Asp sequence (residues 631–632) at the catalytic center.

Functional orientation of VP1

The catalytic center of VP1 lies within a cavity in the center of a cage-like protein.⁴ Four channels connect

the central cavity with the exterior. Structures of template–VP1 complexes and comparison with the reovirus polymerase¹³ show that template inserts through one of these channels and exits through a second, either as a dsRNA genomic product (when the template is the plus strand and the polymerase is in replicative mode) or as a single-stranded RNA (when the template is the minus strand and the polymerase is in transcriptional mode). The remaining two channels appear to allow exit of the plus-strand transcript and entry and exit of small-molecule substrates and products (nucleotides, pyrophosphate, Mg²⁺ ions), respectively.

The position of VP1 within the DLP (Fig. 4) orients the channels so that the template enters from the interior of the particle and the dsRNA exits roughly tangential to the VP2 shell. The putative transcript exit channel opens toward VP2 beneath the position at which two fivefold-related VP2A subunits diverge from each other at the apex of a VP2B subunit, about 30 Å displaced from the 5-fold axis. There is a path from the mouth of the VP1 transcript exit channel toward the fivefold, through which it is likely that transcripts emerge from the DLP.¹⁴ An outward shift of the VP2 pore loop and the helices to either side of it could widen that path. Only one of the five VP2A pore loops need undergo this shift; thus, it might not be evident in the density. There are no strong density features that we can ascribe to VP3, which must intercept the 5' end of the nascent transcript before it exits the DLP.

Discussion

The 11 dsRNA genome segments and the 11–12 copies of VP1 and VP3 pack tightly and efficiently into the DLP interior. Their organization must meet several very restrictive functional requirements. (1) Particle assembly packages one copy each of the 11 capped plus-sense RNA segments and discriminates against non-viral RNAs. (2) Tight packing of the dsRNA within the DLP requires that it coils efficiently. Concentric, low-resolution, internal density layers suggest that each dsRNA segment coils independently around a fivefold hub. (3) Each genome segment undergoes multiple rounds of transcription; the corresponding template strand must therefore pass through a polymerase many times. (4) The capped transcripts emerge from the DLP at or near fivefold positions. The orientation and position of VP1 within the VP2 shell, as described here, adds to our understanding of each of these requirements.

DLP assembly

Association of 10 VP2 subunits (5 VP2A and 5 VP2B, in a 5-fold-symmetric heterodecamer) with

VP1, VP3 and a segment of viral RNA initiates DLP assembly.^{2,3} The N-terminal arms of VP2 are necessary for inclusion of VP1.¹¹ An empty DLP-like particle, lacking VP1, VP3 and RNA, assembles from VP2 (whether full length or with truncated arms) and VP6 alone.^{15,16} Incorporation of RNA, VP1 and VP3 into the assembling particle thus depends on the VP1–VP2 interactions described above, on RNA recruitment by VP1 and probably on association of VP1 with VP3. Recognition by VP1 of a conserved sequence element at the 3' end of plus-sense RNA can account for discrimination against non-viral RNA during packaging,⁴ but it cannot by itself account for selection of 11 distinct RNA segments. The latter process is likely to be encoded in a set of RNA–RNA recognition events not yet evident from the segment sequences alone.

Ten VP2 N-terminal arms project toward each VP1, of which three (two from VP2A subunits and one from a VP2B subunit) appear from density features to interact with the distinct VP1 surfaces against which they lie (Fig. 4). There may be additional arm–VP1 contacts from some of the other VP2 subunits in the heterodecamer; some sort of interaction seems likely from the disposition of the various VP2 N-terminal polypeptide segments in the vicinity of a single VP1.

RNA coiling

The most efficient configuration for tightly packed dsRNA (or any stiff but bendable rod) within a roughly spherical cavity is a more or less regular coil, with local close packing of adjacent segments.^{2,17,18} Low-resolution maps of the rotavirus DLP show layers of density concentric with the inner surface of the VP2 shell, becoming less pronounced toward the interior of the particle² (see also Fig. 2). Earlier analyses of orbivirus and reovirus cores showed similar features.^{19,20} The layers of density avoid completely a volume around the fivefold, extending inward about 75 Å from the VP2 shell. Were RNA wrapped tightly around the single VP1 at each vertex, the density layers would continue into the hub region, overlapping the VP1 density (except in the volume close to the axis, to which VP1 in any of its five equivalent orientations will contribute). VP2 N-terminal arms and VP3 probably fill the 80% of the peri-fivefold region not accounted for by the single VP1. The volume that excludes the RNA density layers could accommodate most or all of these protein components. The clarity of the VP1 density features outside the central region of VP1–VP1 overlap (Fig. 2) suggests, however, that any contributions from VP2 arms or from VP3 create a roughly continuous background—in other words, that neither VP3 nor any ordered segment of a VP2 arm has a fixed position relative to VP1.

The first round of RNA synthesis, which completes DLP assembly in the cytosol, generates dsRNA from the initially incorporated plus-strand RNA. The channel in VP1 for exit of dsRNA opens in a direction tangential to the inner surface of the VP2 shell (Fig. 4c and d). Thus, the polymerase in replicase mode emits its product in the orientation in which it will coil. The orientation of the polymerase suggests that it could assist this coiling, by counter-rotating as the dsRNA emerges and switching from one fivefold-related position to another. The last nucleotides of the plus strand to pass through the template channel are at the capped 5' end. The dsRNA exit channel, through which the cap then re-emerges, is only about 10 Å from the cap-binding site on the VP1 surface.⁴ Capture of the 5' cap can hold the complementary 3' end of the newly synthesized minus strand close to the template entrance channel, through which it must pass to initiate transcription (Fig. 4d).

Transcription

Release of the DLP during viral entry allows transcription to begin. The observed outward displacement of the entire transcriptional complex when the outer layer dissociates (Fig. 3a) probably contributes to activation of the polymerase. The conformational change in VP2 is not an expansion of the entire shell: only the parts of VP2A that surround the particle 5-fold axis (the "apical region") move outward. Therefore, the surface against which VP1 packs changes in contour during the TLP-to-DLP transition. Our current cryoEM reconstructions are not sufficiently accurate, however, to show changes in VP1 that might have occurred in response to the changes in VP2. We therefore cannot rule out the possibility that activation is merely a consequence of "unplugging" the transcript exit route.

During successive rounds of transcription, the 3' end of template (minus) strand must remain close to the polymerase so that it can reenter the template channel when a transcript is complete. We have proposed previously, for both reovirus¹³ and rotavirus⁴ polymerases, that retention of the 5' end of the plus strand during the entire transcription process prevents the 3' end of the minus strand from "getting lost" in the tightly packed interior of the DLP.

VP1 is evidently well anchored in the non-transcribing DLP, as the density for the non-overlapped regions is relatively well defined (Fig. 3), even at 20% effective occupancy. During transcription, the template feeds into the polymerase more or less axially (from the interior of the particle) but exits laterally, parallel with the VP2 inner surface. As we suggest above for the replication step, backward thrust on VP1 from the exiting minus strand might loosen its attachment or cause it to rotate in the direction opposite to that of the emerging template,

with potential reattachment at any of the fivefold equivalent positions.

Comparison with reovirus

In their analysis of both inner cores and intact virions from an orthoreovirus, Zhang *et al.* assigned to fivefold proximal density a copy of the polymerase, $\lambda 3$ (the VP1 equivalent), in an orientation very similar to the one we have determined here.⁹ The sites of nascent mRNA capping of orthoreoviruses are in the "turrets" (protein $\lambda 2$) that project from the shell layer, rather than on a protein within it. Zhang *et al.* suggested that passage of the transcript into the turrets might be through a gap somewhat displaced from the fivefold. Careful inspection of the full atomic model of a non-transcribing core suggests that the gap at that location is largely filled by side chains, but a recent cryoEM structure of a transcribing cypovirus (like reovirus, a turreted dsRNA virus, with capping enzyme active sites facing the interior of the turrets) shows an outward displacement of the apical region of the shell protein, very similar to the conformational change in VP2A that accompanies release of VP7.²¹ The displacement opens the peripentadal gap, and the reconstruction shows some evidence that the transcript does indeed pass through it into the lumen of the turret. Thus, despite differences in the location of their capping activities, the polymerases of several classes of dsRNA viruses appear to have nearly identical functional orientations, linked to their roles in both replication and transcription.

Materials and Methods

Fitting VP1 into a recalculated DLP cryoEM density map

CryoEM images of the rotavirus DLP used in this work were the same as those used previously.^{5,6} A new reconstruction was calculated using SAFs²² and fast projection matching.²³ These two methods can together determine, quickly and accurately, the orientation and center of each particle. Use of SAFs (formally equivalent to Klug's "icosahedral harmonics"^{24,25}) produces three-dimensional (3D) reconstructions with excellent signal-to-noise ratio. Application of these methods to the rotavirus DLP images is described elsewhere.⁶ A total of 7000 of the 18,125 images available in the full DLP data set were used to compute the 3D reconstruction, with resolution estimated by FSC (Fourier shell correlation) to be between 5.6 Å (0.5 criterion) and 4.2 Å (0.143 criterion).⁶ Some high-resolution features can be recognized in non-overlapping zones (Fig. 3a). The fit of the atomic model into the 3D reconstruction was performed using the program URO and its graphical interface VEDA.²⁶ The fitting procedure took into account the difference between the densities associated to each protein given the symmetry mismatch. The Fourier coefficients of VP1 were downweighted by a factor

of 5 in order to prevent VP1 from being “attracted” by the stronger density of the VP2/VP6 layer during the fit. The atomic model of VP1 was placed interactively into the reconstruction with the program PyMOL6 (PyMOL Molecular Graphics System, Version 1.3, Schrödinger, LLC), guided by the well-defined sausage-shaped densities shown in Figs. 2 and 3. The positions of the models were then optimized maximizing the correlation coefficient with the 3D reconstruction, taking into account the icosahedral symmetry and using data to 6 Å. The fit produced a final correlation coefficient of 0.7.

Fitting VP1 into the DLP X-ray density map

The initial identification of features, described in the text, was performed using the program O²⁷ to visualize map and coordinates. Rigid-body refinement was carried out with CNS,²⁸ using the refined models of VP2 and VP6. VP1 was trimmed to exclude obvious overlaps with VP2. The occupancy of VP1 was set to 0.2 to account for the presence of only one VP1 at each 5-fold axis. VP1 is too small a fraction of the total asymmetric unit to contribute noticeably to the working or free *R*-factor in crystallographic refinement.

Accession codes

The atomic model of VP1 attached to capsid inner core has been deposited in the Protein Data Bank with accession codes 4AU6 (EM) and 4F5X (X-ray). The DLP cryoEM map calculated with SAFs has been deposited in the 3D EM database under accession number EMD-2100. The DLP and TLP cryoEM maps calculated with FREALIGN have been deposited previously (EMD-1460 and EMD-5199, respectively).

Acknowledgements

We thank Michael Plevin, Stephen Cusack, Irina Gutsche, Jorge Navaza, Rob Ruigrok and Guy Schoehn for discussion and advice and the European Molecular Biology Laboratory Grenoble for financial support and computational resources. We also acknowledge National Institutes of Health grants CA-13202 (to S.C.H.) and GM-62580 (to N.G. and S.C.H.). S.C.H. and N.G. are investigators in the Howard Hughes Medical Institute.

Received 15 May 2012;

Received in revised form 7 October 2012;

Accepted 11 October 2012

Available online 23 October 2012

Keywords:

virus;
electron cryomicroscopy;
single-particle analysis;
double-stranded RNA

Present addresses: L. F. Estrozi, Institut de Biologie Structurale, 41 Rue Jules Horowitz, Grenoble F-38027, France; E. C. Settembre, Novartis Vaccines and Diagnostics, Cambridge, MA 02139, USA; G. Goret, European Synchrotron Radiation Facility, 6 Rue Jules Horowitz, 38000 Grenoble, France; B. McClain, Vertex Pharmaceuticals, Cambridge, MA 02139, USA; X. Zhang, University of California Los Angeles, Los Angeles, CA 90095, USA; J. Z. Chen, Department of Biology, Massachusetts Institute of Technology, Cambridge, MA 02139, USA.

Abbreviations used:

dsRNA, double-stranded RNA; DLP, double-layered particle; cryoEM, electron cryomicroscopy; TLP, triple-layered particle; SAF, symmetry-adapted function; EM, electron microscopy; 3D, three-dimensional.

References

- Estes, M. K. & Kapikian, A. Z. (2007). Rotaviruses. In *Fields Virology* (Knipe, D. M. & Howley, P. M., eds), pp. 1918–1974., 5th ed Lippincott, Williams & Wilkins, Philadelphia, PA.
- McClain, B., Settembre, E., Temple, B. R., Bellamy, A. R. & Harrison, S. C. (2010). X-ray crystal structure of the rotavirus inner capsid particle at 3.8 Å resolution. *J. Mol. Biol.* **397**, 587–599.
- Gallegos, C. O. & Patton, J. T. (1989). Characterization of rotavirus replication intermediates: a model for the assembly of single-shelled particles. *Virology*, **172**, 616–627.
- Lu, X., McDonald, S. M., Tortorici, M. A., Tao, Y. J., Vasquez-Del Carpio, R., Nibert, M. L. *et al.* (2008). Mechanism for coordinated RNA packaging and genome replication by rotavirus polymerase VP1. *Structure*, **16**, 1678–1688.
- Zhang, X., Settembre, E., Xu, C., Dormitzer, P. R., Bellamy, R., Harrison, S. C. & Grigorieff, N. (2008). Near-atomic resolution using electron cryomicroscopy and single-particle reconstruction. *Proc. Natl Acad. Sci. USA*, **105**, 1867–1872.
- Estrozi, L. F. & Navaza, J. (2010). Ab initio high-resolution single-particle 3D reconstructions: the symmetry adapted functions way. *J. Struct. Biol.* **172**, 253–260.
- Chen, J. Z., Settembre, E. C., Aoki, S. T., Zhang, X., Bellamy, A. R., Dormitzer, P. R. *et al.* (2009). Molecular interactions in rotavirus assembly and uncoating seen by high-resolution cryo-EM. *Proc. Natl Acad. Sci. USA*, **106**, 10644–10648.
- Settembre, E. C., Chen, J. Z., Dormitzer, P. R., Grigorieff, N. & Harrison, S. C. (2010). Atomic model of an infectious rotavirus particle. *EMBO J.* **30**, 408–416.
- Zhang, X., Walker, S. B., Chipman, P. R., Nibert, M. L. & Baker, T. S. (2003). Reovirus polymerase λ 3 localized by cryo-electron microscopy of virions at a resolution of 7.6 Å. *Nat. Struct. Biol.* **10**, 1011–1018.
- Navaza, J., Lepault, J., Rey, F. A., Alvarez-Rua, C. & Borge, J. (2002). On the fitting of model electron densities into EM reconstructions: a reciprocal-space formulation. *Acta Crystallogr., Sect. D: Biol. Crystallogr.* **58**, 1820–1825.

11. Zeng, C. Q., Estes, M. K., Charpilienne, A. & Cohen, J. (1998). The N terminus of rotavirus VP2 is necessary for encapsidation of VP1 and VP3. *J. Virol.* **72**, 201–208.
12. Patton, J. T. & Gallegos, C. O. (1990). Rotavirus RNA replication: single-stranded RNA extends from the replicase particle. *J. Gen. Virol.* **71**, 1087–1094.
13. Tao, Y., Farsetta, D. L., Nibert, M. L. & Harrison, S. C. (2002). RNA synthesis in a cage—structural studies of reovirus polymerase λ 3. *Cell*, **111**, 733–745.
14. Lawton, J. A., Estes, M. K. & Prasad, B. V. (1997). Three-dimensional visualization of mRNA release from actively transcribing rotavirus particles. *Nat. Struct. Biol.* **4**, 118–121.
15. Crawford, S. E., Labbe, M., Cohen, J., Burroughs, M. H., Zhou, Y. J. & Estes, M. K. (1994). Characterization of virus-like particles produced by the expression of rotavirus capsid proteins in insect cells. *J. Virol.* **68**, 5945–5952.
16. Libersou, S., Siebert, X., Ouldali, M., Estrozi, L. F., Navaza, J., Charpilienne, A. *et al.* (2008). Geometric mismatches within the concentric layers of rotavirus particles: a potential regulatory switch of viral particle transcription activity. *J. Virol.* **82**, 2844–2852.
17. Earnshaw, W. C. & Harrison, S. C. (1977). DNA arrangement in isometric phage heads. *Nature*, **268**, 598–602.
18. Harrison, S. C. (1980). Molecular packing of nucleic acids in spherical viruses. In *Biological Recognition and Assembly* (Eisenberg, D. S., Lake, J. A. & Fox, C. F., eds), Alan R. Liss, New York, NY.
19. Gouet, P., Diprose, J. M., Grimes, J. M., Malby, R., Burroughs, J. N., Zientara, S. *et al.* (1999). The highly ordered double-stranded RNA genome of bluetongue virus revealed by crystallography. *Cell*, **97**, 481–490.
20. Reinisch, K. M., Nibert, M. L. & Harrison, S. C. (2000). Structure of the reovirus core at 3.6 Å resolution. *Nature*, **404**, 960–967.
21. Yang, C., Ji, G., Liu, H., Zhang, K., Liu, G., Sun, F. *et al.* (2012). Cryo-EM structure of a transcribing cypovirus. *Proc. Natl Acad. Sci. USA*, <http://dx.doi.org/10.1073/pnas.1200206109>.
22. Navaza, J. (2003). On the three-dimensional reconstruction of icosahedral particles. *J. Struct. Biol.* **144**, 13–23.
23. Estrozi, L. F. & Navaza, J. (2008). Fast projection matching for cryo-electron microscopy image reconstruction. *J. Struct. Biol.* **162**, 324–334.
24. Finch, J. T. & Holmes, K. C. (1967). Structural studies of viruses. In *Methods in Virology* (Maramarsoch, K. & Koprowski, H., eds), pp. 352–474, Academic Press, New York, NY.
25. Jack, A. & Harrison, S. C. (1975). On the interpretation of small-angle X-ray solution scattering from spherical viruses. *J. Mol. Biol.* **99**, 15–25.
26. Siebert, X. & Navaza, J. (2009). UROX 2.0: an interactive tool for fitting atomic models into electron-microscopy reconstructions. *Acta Crystallogr., Sect. D: Biol. Crystallogr.* **65**, 651–658.
27. Jones, T. A., Zou, J. Y., Cowan, S. W. & Kjeldgaard, M. (1991). Improved methods for building protein models in electron density maps and the location of errors in these models. *Acta Crystallogr., Sect. A: Found. Crystallogr.* **47**, 110–119.
28. Brunger, A. T., Adams, P. D., Clore, G. M., DeLano, W. L., Gros, P., Grosse-Kunstleve, R. W. *et al.* (1998). Crystallography & NMR system: a new software suite for macromolecular structure determination. *Acta Crystallogr., Sect. D: Biol. Crystallogr.* **54**, 905–921.